JGR Oceans

RESEARCH ARTICLE
10.1029/2022JC019493

Special Section:
Forcing, response, and impacts of coastal storms in a changing climate

Characteristics of Storm Surge Events Along the North-East Atlantic Coasts

Lucia Pineau-Guillou[1], Jean-Marc Delouis[2], and Bertrand Chapron[1]

[1]IFREMER, Laboratoire d'Océanographie Physique et Spatiale, UMR 6523 (IFREMER, CNRS, IRD, UBO), IUEM, Brest, France, [2]CNRS, Laboratoire d'Océanographie Physique et Spatiale, UMR 6523 (IFREMER, CNRS, IRD, UBO), IUEM, Brest, France

Key Points:

- A new method ECHAR is proposed to characterize the dynamics of typical storm surge events
- Storm surge events display a slow-time and a fast-time component lasting about 16 and 1.7 days respectively
- The wind stress mostly contributes to the fast-time component whereas the atmospheric pressure contributes to both

Correspondence to:
L. Pineau-Guillou,
lucia.pineau.guillou@ifremer.fr

Citation:
Pineau-Guillou, L., Delouis, J.-M., & Chapron, B. (2023). Characteristics of storm surge events along the North-East Atlantic coasts. *Journal of Geophysical Research: Oceans*, *128*, e2022JC019493. https://doi.org/10.1029/2022JC019493

Received 15 NOV 2022
Accepted 11 APR 2023

Abstract Storm surges are often characterized in terms of magnitude, duration and frequency. Here, we propose a novel statistical method to help characterize the full dynamics of storm surge events. The method, called ECHAR, is based on techniques already successfully applied in astrophysics. Analysis of 20 tide gauges in the North-East Atlantic consistently reveals that storm surge events display two distinctive components, a slow-time background Gaussian structure and a fast-time Laplace structure. Each of these structures can be reduced to its duration and amplitude. For large events, occurring 5 times per winter, the slow-time structure lasts around 16 days, varying from 9 days in the South to 45 days in the North (Baltic Sea), with almost the same amplitude at all the stations (around 0.17 m). The fast-time structure lasts around 1.7 days at all the stations, but its amplitude greatly varies, from 0.1 m in the South to 1.6 m in the North Sea. The wind stress contributes mostly to the fast-time component of the storm surge event, whereas the atmospheric pressure contributes to both components. The proposed ECHAR method, helping to characterize extreme events, can be applied anywhere else in the global ocean, for example, where tropical storm surges occur.

Plain Language Summary Storm surges are an increase of the sea level, due to low atmospheric pressure and strong winds during storms. We propose a new method, to characterize storm surge events in the North-East Atlantic. We consider the largest events, that happen only 5 times per winter. A typical storm surge event is a gradual slow increase and then decrease of the water level, over a period of few days to few weeks, from 9 days in the South to 45 days in the North (Baltic Sea). In addition, when the storm is at its peak, the water level suddenly rises, due to the passage of strong winds. This rise occurs on a very short period, only few hours, and can be locally very large (more than 1 m in the North Sea).

1. Introduction

Storm surges are the sea level response to the passages of extreme weather events, generated by low atmospheric pressure systems and strong winds, crossing northwestern Europe. Storm surges may impact severely coastal areas, causing large flooding. For example, in the North Sea, during the 1953 great storm, storm surges larger than 3 m flooded the Netherlands and southeast England, causing more than 2000 deaths (Choi et al., 2018; Wolf & Flather, 2005). It is essential to better characterize these extreme events, in order to investigate if future events will become more or less severe, in a warming climate (IPCC, 2021).

There are different ways to define storm surge events, and investigate their changes. (a) A common approach is to select values over a percentile. For example, Marcos and Woodworth (2017) characterized extreme surges as the surges exceeding the 99th percentile of the hourly time series, and respecting an independence criteria of 3 days. Since 1960 in the North Atlantic, these authors found mostly negative trends for annual 99th percentile along the Atlantic coasts of Southern Europe, and no significant trends elsewhere. Reinert et al. (2021) also investigated changes in the annual 99th percentile of surge levels at Brest (France), but did not report any significant trend over the period 1846–2018. (b) Another classical approach is to define extremes in terms of return level, that is, an estimation of the level that is expected to occur, for instance, once every 10 years, on average. Extreme value distributions, such as Generalized Extreme Values (GEV) or General Pareto Distribution (GPD), are fitted on extreme surges, and return levels are estimated (Coles, 2001). Extreme surges are selected as values over a threshold for the GPD, and maxima over a given period for the GEV. Following this approach, Vousdoukas et al. (2016) applied a GPD on surges exceeding a given threshold, to estimate storm surge levels for different return periods in Europe. At New-York, Talke et al. (2014) applied a GEV on the annual largest surges, to estimate the 10 years

storm surge return level, over a 37 years sliding window. These authors found that the 10 years storm surge amplitude has increased since the mid-19th century. In the North Atlantic, Marcos and Woodworth (2017) applied a GEV on the five annual largest surges. These authors introduced a linear trend in the location parameter (one of the parameters of the GEV), to investigate possible trends in the storm surges. Since 1960, 60% of the tide gauges did not show significant trends in the location parameter.

Beyond magnitude, storm surge events can also be investigated in terms of duration. Haigh et al. (2010) defined the duration as the annual number of hours for which the storm surges were above a given threshold. In the English Channel, no significant long-term changes were found at any of the study sites, over the period 1900–2006. Similarly, Cid et al. (2016) considered the duration of each storm surge event, as the number of hours the level is above a given threshold. Fitting a non stationary GPD on the sample of duration of the independent events, these authors found in Southern Europe, from 1948 to 2013, some positive trends in certain Mediterranean areas. Durations of extreme events increased at a rate of 0.5–1.5 hr/year.

Storm surge events can also be investigated in terms of frequency. A common approach is to count the number of events per year exceeding a threshold (Haigh et al., 2010; Marcos et al., 2015) or to use the Poisson process to study the occurrence rate of the exceedances above a threshold (Cid et al., 2016). At global scale, the frequency of storm surges show spatially coherent decadal to multidecadal variations, but no clear centennial trends (Marcos et al., 2015).

Finally, storm surge events can also be investigated in terms of timing, that is, when they mostly occur. Along the European coasts, extreme surges mostly occur in December or January (Menéndez & Woodworth, 2010). At Brest (France), Reinert et al. (2021) reported a shift of 3 weeks in the storm surge timing, extreme events occurring mid-December in 2000, rather than beginning of January in the 1950s. Recently, at larger scale, Roustan et al. (2022) showed that extreme surge events occurred about 4 days/decade later in northern Europe, and 5 days/decade earlier in southern Europe, still on the 1950–2000 period.

Storm surge events are thus often characterized by their magnitude, duration (time over a threshold), frequency (how often they occur) and timing (when they occur). But very few studies investigate the full dynamics of a typical storm surge event, from the time the pressure starts to decrease, few days before the maximum storm surge, to the moment the atmospheric pressure reaches back an average condition. This has already been done when investigating individual events, for example, Xynthia storm (Bertin et al., 2014; Pineau-Guillou et al., 2012), Xaver storm (Dangendorf et al., 2016), for process understanding or model validation (Pineau-Guillou et al., 2020), but this has rarely been done in a more statistical approach.

The main objectives of the paper are (a) to characterize the full dynamics of storm surge events (b) to reduce a storm surge event to few characteristic parameters (c) to interpret these parameters, in link with the atmospheric pressure and the wind stress. The study focuses on the North-East Atlantic.

The paper is organized as follows. The next section describes the data used in this study: the tide gauges and atmospheric reanalysis. The following section presents a new method, to extract the typical shape of a storm surge event from surge time series. We then present the results: the patterns of the storm surge events in the North-East Atlantic, and their characteristic parameters. Finally, we discuss the role of the atmospheric pressure and the wind stress in the storm surge event.

2. Data

2.1. Sea Level Data

We used tide gauge data from GESLA (Global Extreme Sea Level Analysis) Version 3 (Caldwell et al., 2015; Haigh et al., 2021; Woodworth et al., 2017). This data set provides high-frequency (i.e., hourly or subhourly) sea level observations at 5119 tide gauges worldwide. The longest record is Olands Norra Udde (Sweden) with 168 years between 1851 and 2021, and the second longest record is Brest (France), with 165 years between 1846 and 2021.

We selected coastal stations, with at least 50 years of data. This criteria led to a large number of tide gauges (almost 100), and we selected 20 of them regularly distributed along the North-East Atlantic coasts (Figure 1). The time span and length of each station are synthesized in Table 1 (see columns 3 and 4). Note that among the 20 selected stations, only one is slightly shorter than 50 years (La Rochelle, France, 44 years).

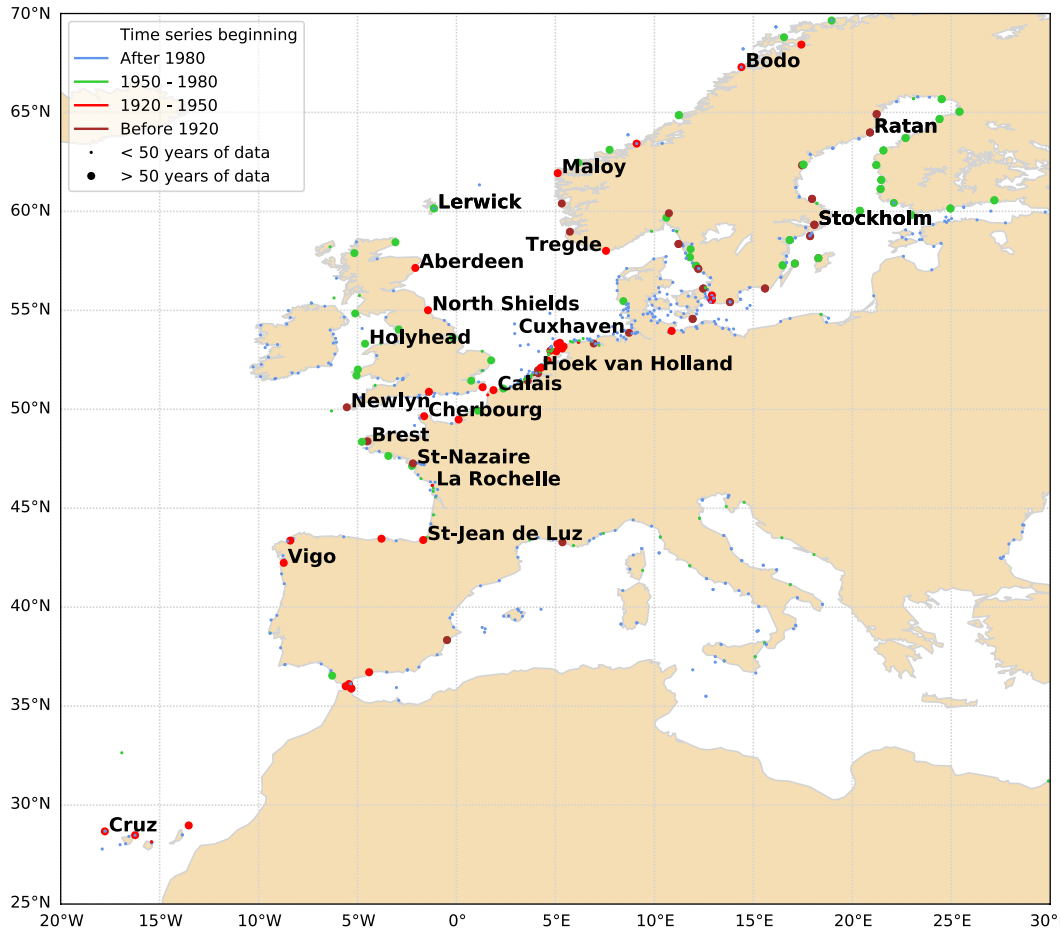

Figure 1. Location of GESLA-3 stations. Tide gauges used in this study are labeled in bold.

We processed the sea level data to compute the hourly surges, removing (a) the tide and (b) the mean sea level from the hourly observations. (a) The tide was computed from a harmonic analysis over the last 20 years of data, using the Tidal ToolBox, developed by LEGOS (Allain, 2021). We chose a long period for the harmonic analysis (20 years, close to the 15 years of Marcos and Woodworth (2017)) rather than a short period (as 1 year in Reinert et al. (2021)), to ensure an accurate predicted tide (Simon, 2007, 2013). The drawback of this method is that any long-term change in tide is not taken into account (Haigh et al., 2019; Pineau-Guillou et al., 2021). However, as we focus on recent data (since 1980, see below), we assume that these changes are small. (b) The mean sea level was removed yearly, to avoid a mean sea level rise signal in the surges (Calafat et al., 2022; Marcos & Woodworth, 2017).

We selected the hourly surges since 1980, rather than since the beginning of the record, for two reasons. The first reason is that recent instruments show less systematic errors (e.g., timing errors) than historic tide gauges. The second reason is that the atmospheric data we use start in 1979 (see next section); starting in 1980 ensures a common period of analysis.

Finally, we obtain the hourly surges at 20 stations, from 1980 to the end of the record (between 2015 and 2021 depending on the station, see Table 1 column 5).

2.2. Atmospheric Data

We used atmospheric data from ERA5 reanalysis, on the period 1979–2021 (Hersbach et al., 2018, 2020). This data set provides hourly 10-m surface winds and sea level pressure at global scale, with a horizontal resolution of 31 km. Note that ERA5 starts in 1950, but only the period 1979 onwards was publicly available at the time of the analysis.

Table 1
Main Features of Tide Gauge Records Used in This Study: Station Name, Time Span, Number of Years With Data, Period Analyzed, and Characteristic Parameters for a Storm Surge Event, Occurring 5 Times per Winter, That Is, Amplitude and Duration of the Slow-Time (Gaussian) Structure and Fast-Time (Laplace) Structure (a_G, a_L, Δt_G, Δt_L)

	Station name	Time span	Nb of years	Period analyzed	a_G (m)	a_L (m)	Δt_G (days)	Δt_L (days)
1	Cruz	1949–2015	56	1980–2015	0.07	0.08	10.0	2.2
2	Vigo	1943–2015	73	1980–2015	0.14	0.23	11.3	2.2
3	St-Jean De Luz	1942–2018	52	1980–2018	0.17	0.12	9.5	2.0
4	La Rochelle	1941–2020	44	1980–2020	0.20	0.35	11.8	1.4
5	St-Nazaire	1821–2020	134	1980–2020	0.19	0.45	12.9	1.3
6	Brest	1846–2021	165	1980–2021	0.18	0.33	14.0	1.5
7	Newlyn	1915–2021	107	1980–2021	0.15	0.32	17.1	1.9
8	Holyhead	1964–2021	51	1980–2021	0.15	0.67	21.0	1.3
9	Cherbourg	1943–2020	50	1980–2020	0.18	0.39	13.7	1.3
10	Calais	1941–2021	56	1980–2021	0.14	0.70	11.1	1.3
11	Hoek van Holland	1900–2018	89	1980–2018	0.15	1.08	14.9	1.8
12	Cuxhaven	1917–2018	102	1980–2018	0.27	1.64	13.1	1.9
13	North Shields	1946–2021	68	1980–2021	0.07	0.83	18.2	1.1
14	Aberdeen	1930–2021	73	1980–2021	0.11	0.66	19.7	1.2
15	Lerwick	1959–2021	63	1980–2021	0.19	0.26	10.3	2.5
16	Tregde	1927–2020	94	1980–2020	0.15	0.44	13.9	1.6
17	Maloy	1943–2020	76	1980–2020	0.21	0.33	14.5	1.9
18	Bodo	1949–2020	71	1980–2020	0.17	0.47	12.0	1.6
19	Stockholm	1889–2021	133	1980–2021	0.19	0.16	28.8	1.8
20	Ratan	1891–2020	130	1980–2020	0.22	0.43	45.1	2.7
	Average				0.17	0.50	16.1	1.7
	Standard deviation				0.05	0.36	8.0	0.4

For each tide gauge, we extracted the atmospheric time series from ERA5 at the nearest ocean grid point.

3. Method

3.1. Extraction of a Typical Storm Surge Event

To help characterize the full dynamics of storm surge events, we adapted a method successfully applied in astrophysics, to identify energetic particle dynamics effects on Planck High Frequency Instrument detectors (Planck Collaboration et al., 2014). The method is based on data reduction, using a 2D histogram, to help highlight repetitive patterns in the signal. Accordingly, the proposed ECHAR (Event CHARacterization) method enables extracting the shape of a typical storm surge event from surge time series.

For method illustration (Figure 2), we apply it to Brest time series, consisting of hourly surges from 1980 to 2020. Only "winter" data are considered ("winter" being from October to March), as extreme surges mostly occur during the winter season. The different ECHAR steps are the following:

- Step 1: select the n (here, $n = 5$) maximum surges per winter (red points on Figure 2a). Considering $n = 5$ events per year is common for extreme values statistical analysis (Marcos & Woodworth, 2017; Vousdoukas et al., 2016). To ensure that each maximum corresponds to a single storm event, a classical independence criterion of 3 days between each of them is considered (Marcos et al., 2015; Marcos & Woodworth, 2017). Note that only a short part (1986–1988) of the time series (1980–2020) is displayed on Figure 2a, to make the figure more readable.
- Step 2: stack the n storm surge events together, by shifting the curves, so that the peak surge of each event (red point on Figure 2a) is now centered on 0 (Figure 2b). We focus on few days (here, 20 days) before and after

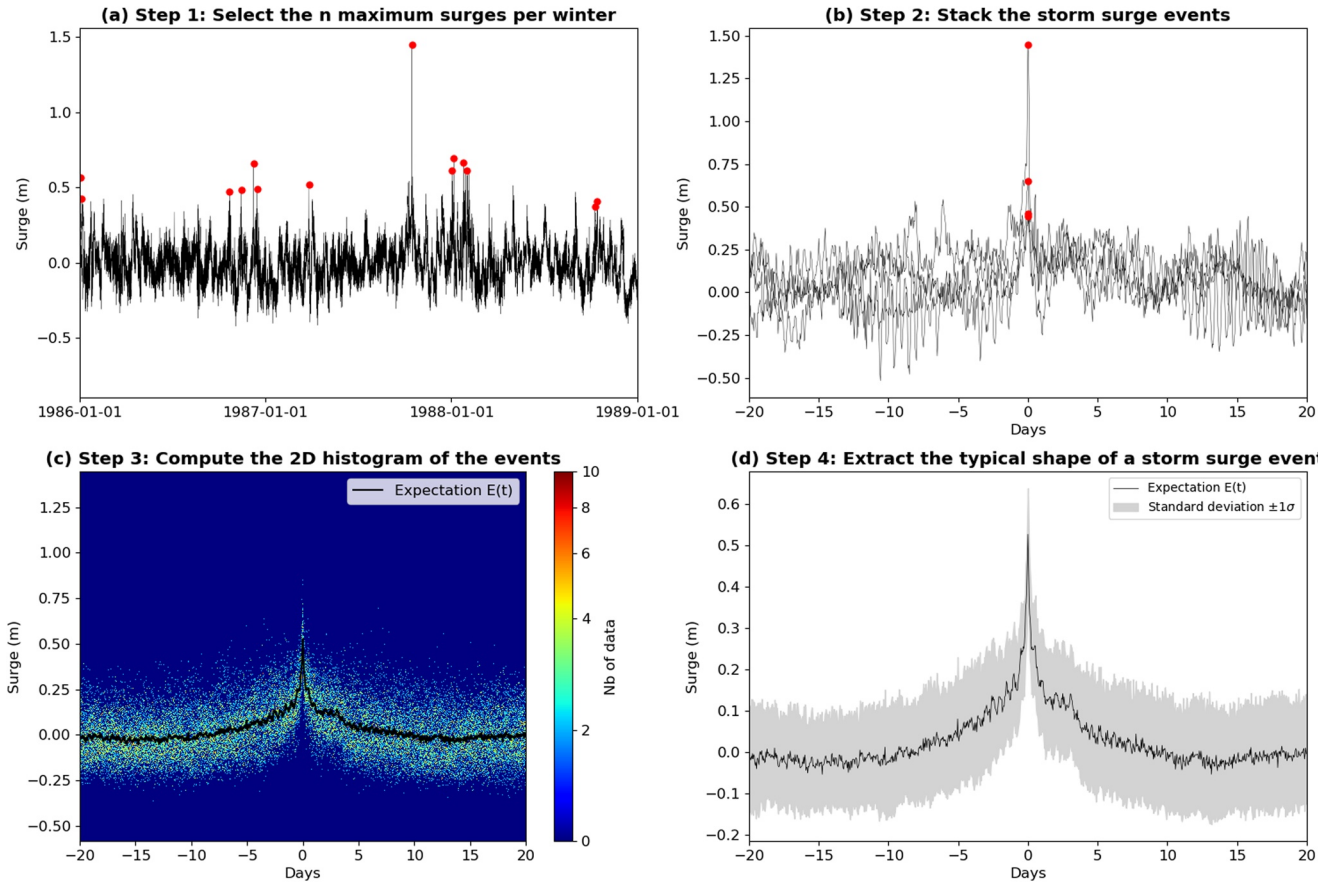

Figure 2. Illustration of the different steps of the ECHAR method, which extracts from a storm surge time series (here, Brest 1980–2020 record) the typical shape of a storm surge event occurring n times a year (here, $n = 5$). Note that only a short part (1986–1988) of the time series (1980–2020) is displayed on (a), to make the figure more readable. The same way, only a small part of the events (4 events) is displayed on (b), to make the figure more readable.

the peak surge. Note that only a small part of the events (4 events) are shown Figure 2b, to make the figure more readable.

- Step 3: compute the 2D histogram of all the events (Figure 2c).
- Step 4: extract the typical shape of a storm surge event (Figure 2d), by computing the expectation $E(t)$ and standard deviation $\sigma(t)$ of the surge probability distribution at each time t_i:

$$E(t_i) = \sum_j x_j P_{ij} \tag{1}$$

$$\sigma(t_i) = \sqrt{\sigma^2} = \sqrt{\sum_j (x_j - E(t_i))^2 P_{ij}} \tag{2}$$

with P_{ij} is the probability to have a surge x_j at the time t_i. The shape of a typical storm surge event corresponds to the expectation $E(t)$ (Figure 2d). The spread around this mean is given through the standard deviation (shaded areas on Figure 2d). The Gaussian approximation is acceptable, as we consider a large number of storm surge events (5 events per year since 1980, i.e., much more than 100 events).

3.2. Characteristic Parameters of a Storm Surge Event

A typical storm surge event $E(t)$ is the combination of two structures, with different time scales: a slow-time structure, and a fast-time structure, more peaked, which is superimposed on the top of the slow-time structure (see the red curve on the top of the black curve in Figure 3). The slow-time structure can be modeled with a

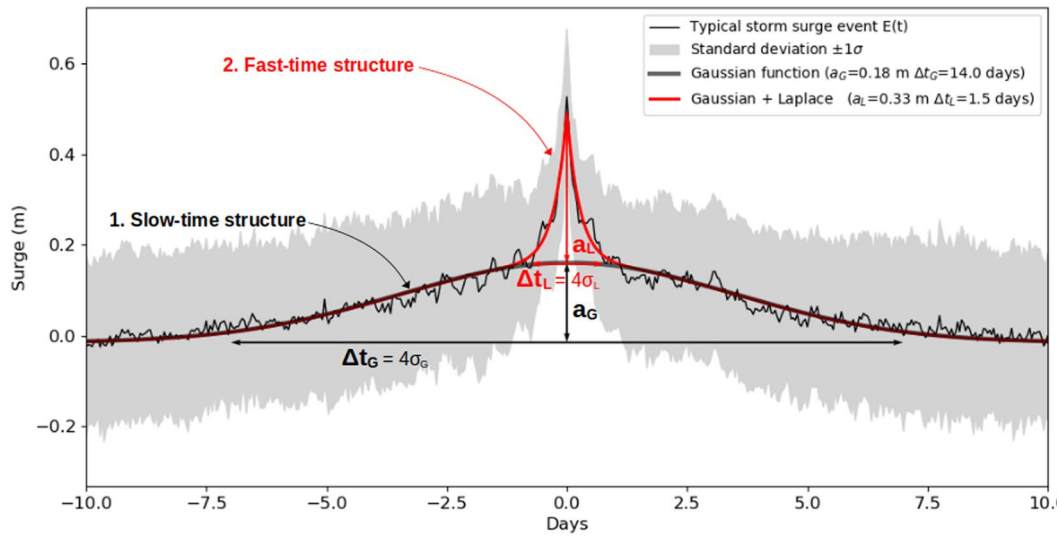

Figure 3. Shape of a typical storm surge event occurring 5 times per year at Brest, and associated characteristic parameters: a_G (Gaussian amplitude), Δt_G (Gaussian duration), a_L (Laplace amplitude) and Δt_L (Laplace duration).

Gaussian function $f_G(t)$, whereas the fast-time structure, more peaked, can be modeled with a Laplace function (also referred as Laplace distribution) $f_L(t)$:

$$\begin{cases} E(t) = f_G(t) + f_L(t) \\ f_G(t) = a_G e^{-(t-\mu_G)^2/2\sigma_G^2} \\ f_L(t) = a_L e^{-\sqrt{2}|t-\mu_L|/\sigma_L} \end{cases} \quad (3)$$

with $E(t)$ a typical storm surge event, $f_G(t)$ and $f_L(t)$ the Gaussian and Laplace functions, a_G, μ_G, $\sigma_G$and a_L, μ_L, σ_L the amplitude, mean and standard deviation of the Gaussian and Laplace functions, respectively. Note that by construction, the mean μ_G and μ_L are close to zero, as all events are centered on zero (see Figure 2b). The Gaussian and Laplace functions can be reduced to their amplitude and duration, the duration being defined as 4 times the standard deviation ($\Delta t = 4\sigma$). This ensures that almost all the storm surges values (95%) are within this duration (i.e., 2 standard deviations of the mean). Finally, a typical storm surge event thus reduces to 4 characteristic parameters:

- a_G: amplitude of the slow-time Gaussian structure,
- a_L: amplitude of the fast-time Laplace structure,
- $\Delta t_G = 4\sigma_G$: duration of the slow-time Gaussian structure,
- $\Delta t_L = 4\sigma_L$: duration of the slow-time Laplace structure.

We estimate the characteristic parameters a_G, a_L, Δt_G,and Δt_L, by fitting a Gaussian and Laplace function (Equation 3) on a typical storm surge event $E(t)$ (Equation 1). Technically, we first fit the Gaussian function, taking care of removing the core of the storm surge event, that is, the day around the peak surge (data from −1 to 1 day). This helps to isolate the slow-time structure component of the signal, avoiding that the fast-time structure influences the slow-time structure in the fit. Once the Gaussian parameters are estimated, we compute the residual removing the Gaussian structure $f_G(t)$ from the surge signal $E(t)$. We then fit the Laplace function $f_L(t)$ on this residual, to estimate the Laplace parameters.

At Brest, the following characteristic parameters are found, for a typical event occurring 5 times per winter: 18 cm and 14 days for the slow-time structure, 33 cm and 1.5 days for the fast-time structure (Figure 3). The peak surge thus reaches around 51 cm, which can be interpreted as the average of the 5 highest storm surges per year over the analyzed period 1980–2020 (the exact value is 54 cm).

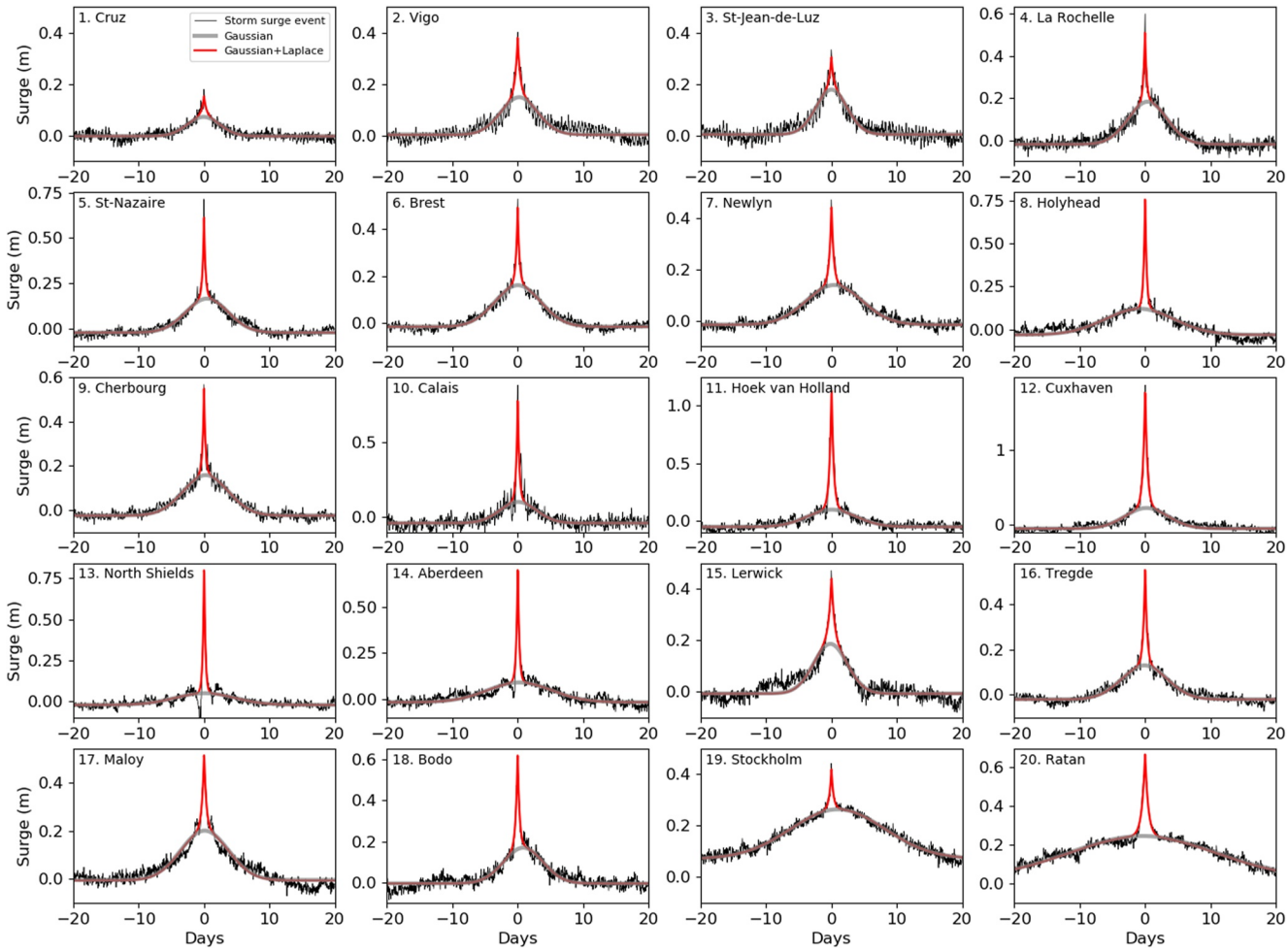

Figure 4. Shape of a typical storm surge event occurring 5 times per winter, at the 20 tide gauges. Observed events are in black, whereas modeled ones (with Gaussian and Laplace functions) are in red.

4. Results

4.1. Patterns of the Storm Surge Events

The ECHAR method is applied at all the stations, located in the North-East Atlantic (Figure 1). Again, the 5 highest winter events were selected over the period 1980–2020 (see the exact period for each station Table 1 column 9). From all these events, the shape of a typical storm event is then extracted (see Figure 2 for the method), and modeled as the combination of a Gaussian and Laplace function (see Figure 3 for an illustration at Brest). The shapes of a typical storm surge event at each station are presented in Figure 4: observed shapes are in black, whereas modeled ones are in red.

The first result is that the Gaussian and Laplace decomposition (Equation 3) very well approximate each typical surge event. The RMSE (Root Mean Square Error) between the observed surge events (in black on Figure 4) and modeled ones (in red on Figure 4) is very small, on average 2 cm, and always smaller than 4 cm. For almost all cases, the peak surge is also well estimated; on average, the differences between the two peak surges (observed and modeled) is very small (−2 cm), the difference being maximum at Calais (–11 cm, see station 10 on Figure 4).

The second result is that the shape of a typical event, occurring 5 times per winter, can be very different depending on the location. The duration of the slow-time structure is much longer in the Baltic Sea than in the North Sea (see the difference of shape between station 12 Cuxhaven in the North Sea, and station 20 Ratan in the Baltic Sea on Figure 4). The peak surge is much larger in the North Sea, than anywhere else, with almost 2 m at station 12 Cuxhaven in the North Sea, whereas only 0.6 m at station 20 Ratan in the Baltic Sea (Figure 4).

Finally, the residual, that is, the difference between observed and modeled storm surge events, is often dominated by some high-frequency oscillations, see for example, station 2 Vigo (Figure 4). The frequency of this signal is close to M_2 tide (the main tidal frequency); its amplitude is quite small, around few centimeters (e.g., 3 cm at Vigo, 5 cm at Calais). These oscillations could have different origins. A significant harmonic component could be missing in the tide prediction. This is unlikely, as we conducted the harmonic analysis on a sufficiently long period (20 years) to ensure an accurate prediction. These oscillations have more likely a physical origin. It could be the signature of tide-surge interaction (Horsburgh & Wilson, 2007). The storm surge increases the water depth h, and then the tide propagation speed $\sqrt{gh}$ where g is the mean gravitational acceleration. As a consequence, a positive surge leads the tide to occur sooner than predicted. The high water can thus be shifted by a few minutes. This small shift between the predicted tide and observed sea level can introduce some oscillations in the surge signal (see Figure 4 in Horsburgh and Wilson (2007)). A periodic signal at M_2 frequency can appear regularly at tide gauges with large tidal range, as for example, Saint-Malo in the English Channel (see Figure 19 in Muller et al. (2014)). The tide-surge interaction can reach locally some tens of centimeters (Idier et al., 2012). Note that studying "skew surges," that is, the difference between the maximum observed sea level and the maximum tide prediction during a tidal cycle (Pugh & Woodworth, 2014), rather than "instantaneous surge," that is, the differences between hourly observed and predicted sea levels (as in this paper) naturally avoids these oscillations. However, investigating skew surges (rather than hourly surges) is not relevant in the context of our study, as the skew surges are computed every 12 hr 25 mn (one point per tidal cycle), and have no high frequency temporal evolution.

4.2. Characteristic Parameters

For all the stations, the characteristic parameters, a_G, a_L, Δt_G, and Δt_L, of a typical storm surge event (occurring 5 times per winter) were estimated (Figure 5 and Table 1).

The first result is that the slow-time Gaussian structure has a longer duration, but smaller amplitude, than the fast-time Laplace structure. On average, the duration is 16 days for the slow-time structure, against 1.7 days for the fast-time one; the amplitude is about 0.17 m for the slow-time structure, against 0.50 m for the fast-time one.

The second result is clearly highlighted on Figure 6 (note that the x-axis is log scale): the duration of the slow-time component (in black on Figure 6) varies greatly, from 9 days at St-Jean de Luz in the South to 45 days at Ratan in the Baltic Sea, whereas its amplitude is almost identical for all the stations (0.17 ± 0.05 m). The long duration of storm surge events in the Baltic Sea is consistent with the previous study from Marcos and Woodworth (2017). These authors defined differently the duration of an event (i.e., number of hours, around the peak of the event, the sea level is above the 99th percentile of total sea levels), but they also found that events were much longer in the Baltic Sea, exceeding 20 hr against less than 5 hr along the North-East Atlantic coasts. For the fast-time component (in red on Figure 6), the duration is almost identical at all the stations (1.7 ± 0.4 days), whereas its amplitude varies greatly, from less than 0.1 m at Cruz (Azores) to 1.6 m at Cuxhaven (North Sea).

4.3. Wind and Atmospheric Pressure Contributions to a Storm Surge Event

The storm surges are generated by atmospheric pressure gradient and wind stress. The wind stress is generally parameterized using the following bulk formula:

$$\tau = \rho_a u_*^2 = \rho_a C_d U_{10}^2 \tag{4}$$

with u_* the friction velocity, C_d the drag coefficient and U_{10} the wind speed at 10 m above the surface. We used a drag formulation as a function of the wind speed (Hellerman & Rosenstein, 1983), to compute the wind stress.

The ECHAR method is applied to the atmospheric pressure and wind stress time series, following the same procedure as for surge time series. We obtain the typical shapes of an atmospheric pressure extreme event (Figure 7b for Brest) and a wind stress event (Figure 7c), the same way we obtained the typical shape of a storm surge event (Figure 7a). Extreme events are still defined as occurring 5 times per winter, and are selected in the vicinity of the storm surge events. We used a 3-day window around the peak surge to detect the timing of the atmospheric extremes (maximum wind stress or minimum atmospheric pressure), as the atmospheric data are not necessarily extremes exactly when the peak surge occurs (i.e., there may be a small time lag).

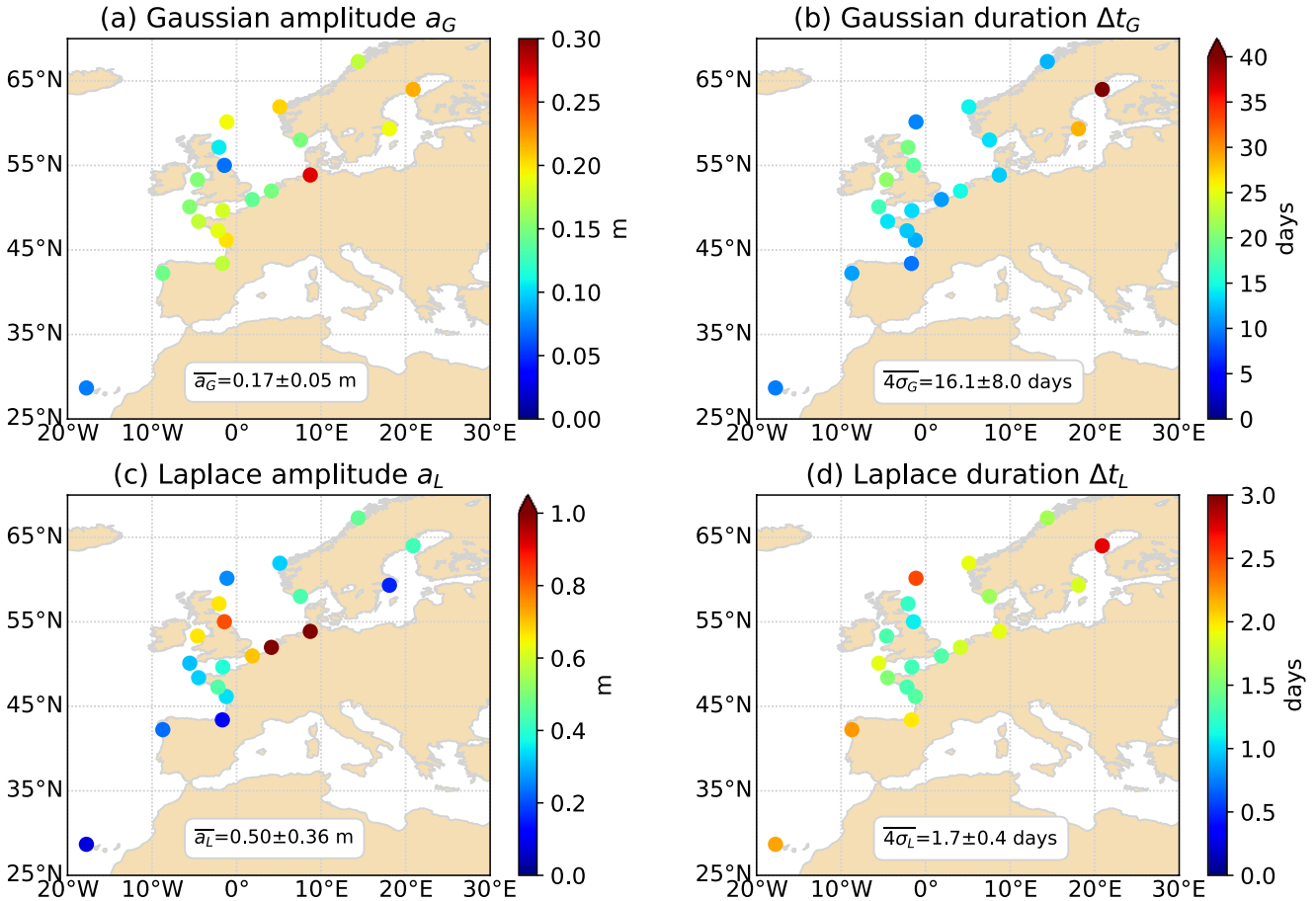

Figure 5. Characteristic parameters of a typical storm surge event occurring 5 times per winter: (a) amplitude a_G (b) duration Δt_G of the slow-time Gaussian structure (c) amplitude a_L (d) duration Δt_L of the fast-time Laplace structure.

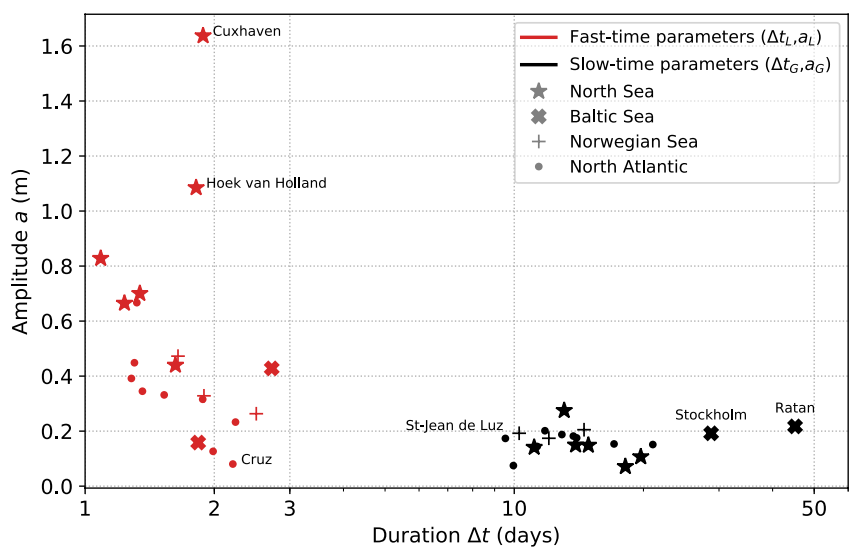

Figure 6. Characteristic parameters of a typical storm surge event occurring 5 times per winter at the 20 tide gauges: duration and amplitude of the Laplace fast-time structure (Δt_L, a_L, in red) and Gaussian slow-time structure (Δt_G, a_G, in black).

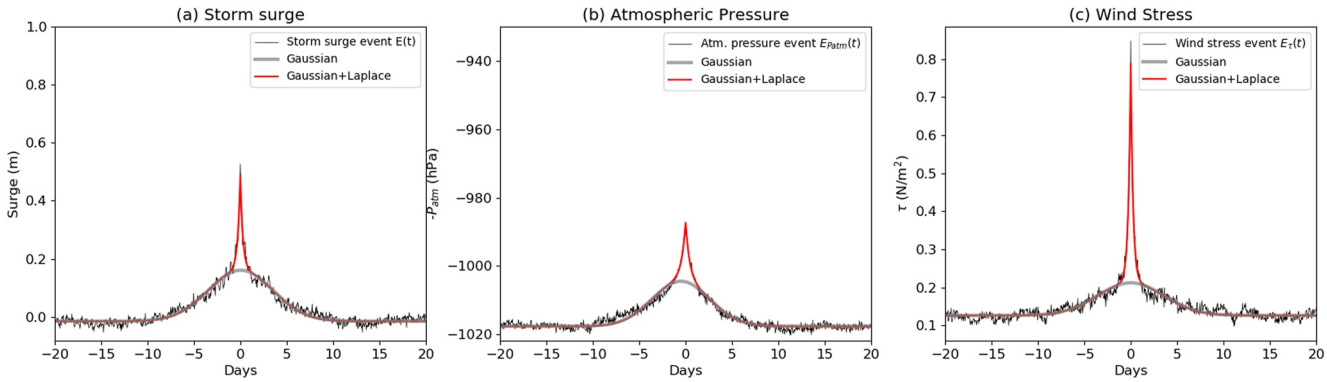

Figure 7. Shape of a typical (a) storm surge event (b) extreme atmospheric pressure event and (c) extreme wind stress event at Brest. Observed events are in black, whereas modeled ones (with Gaussian and Laplace functions) are in red.

Typical events of atmospheric pressure and wind stress are also a combination of two structures, that is, a slow-time Gaussian and fast-time Laplace component (see the gray and red curves on Figure 7). At all the stations, wind stress events are mainly reduced to its fast-time component, with similar duration of around 1.5 days. The contribution of the fast-time amplitude to the peak of the wind stress event (i.e., $a_L/(a_G + a_L)$) is of 87% at Brest, and 90% on average at all the stations. In other words, the wind stress mainly contributes to the fast-time structure of the storm surge, whereas atmospheric pressure contributes to both structures.

To analyze the relative contribution of the atmospheric pressure and the wind stress in a typical storm surge event, we thus model the storm surge event as a multiple linear regression of the driving events, that is, the atmospheric pressure and the wind stress events:

$$E_{surge}(t) = \alpha E_{Patm}(t) + \beta E_\tau(t) \tag{5}$$

with $E_{surge}(t)$, $E_{Patm}(t)$, and $E_\tau(t)$ the storm surge, atmospheric pressure and wind stress events, computed using the ECHAR method (see Figure 7, for the example at Brest). Note that in Equation 5, $E_{Patm}(t)$ and $E_\tau(t)$ are normalized (the average is removed, and the result is divided by the maximum), to ensure that they vary between 0 and 1. This way, the ratio between β and $\alpha + \beta$ gives the contribution of the wind stress in the storm surge event:

$$r_\tau = \frac{\beta}{\alpha + \beta} \tag{6}$$

The storm surge events observed and modeled from the drivers (atmospheric pressure and wind stress) at all the stations are presented in Figure 8. Except in the Baltic Sea (see stations 19 and 20, Stockholm and Ratan), the linear combination of atmospheric pressure and wind stress events very well approximate the storm surge event, at all the stations. On average, the RMSE between the multiple linear model and the storm surge event is of only 1 cm. The peak surge is also correctly modeled, despite a slightly underestimation (–2 cm in average). The maximum of underestimation is found at Stockholm (–12 cm). Some stations display an asymmetry in the storm surge signal, see for example, station 8 Holyhead or station 18 Bodo (Figure 8). This asymmetry is very well captured by the model. Note that in the following, we will not consider Stockholm and Ratan, the model being not able to correctly reproduce a storm surge event at these two stations located in the Baltic Sea.

The wind stress contribution in the storm surge event (r_τ, see Equation 6) is presented on Figure 9. The atmospheric pressure is the main driver of storm surge events at most of the stations (12 among 18), all located along the Atlantic coasts or the Norwegian Sea. The wind stress is the main driver at the remaining stations (6 stations among 18), all located in the North Sea or in the Irish Sea. On average, the wind stress contribution to the storm surge event is of 43%, and greater than 50% at around half of the stations (11 stations among 20). The highest contributions, in the order of 90%, are obtained in the North Sea, with for example, a wind stress contribution of 90% at North Shields and 99% at Cuxhaven. These high values in the North Sea can be explained by two reasons: (a) the proximity of the storm tracks, which implies higher wind values than in the South (b) the shallow waters of the North Sea, which increase the wind stress effect through effective Ekman transport. In the classical shallow

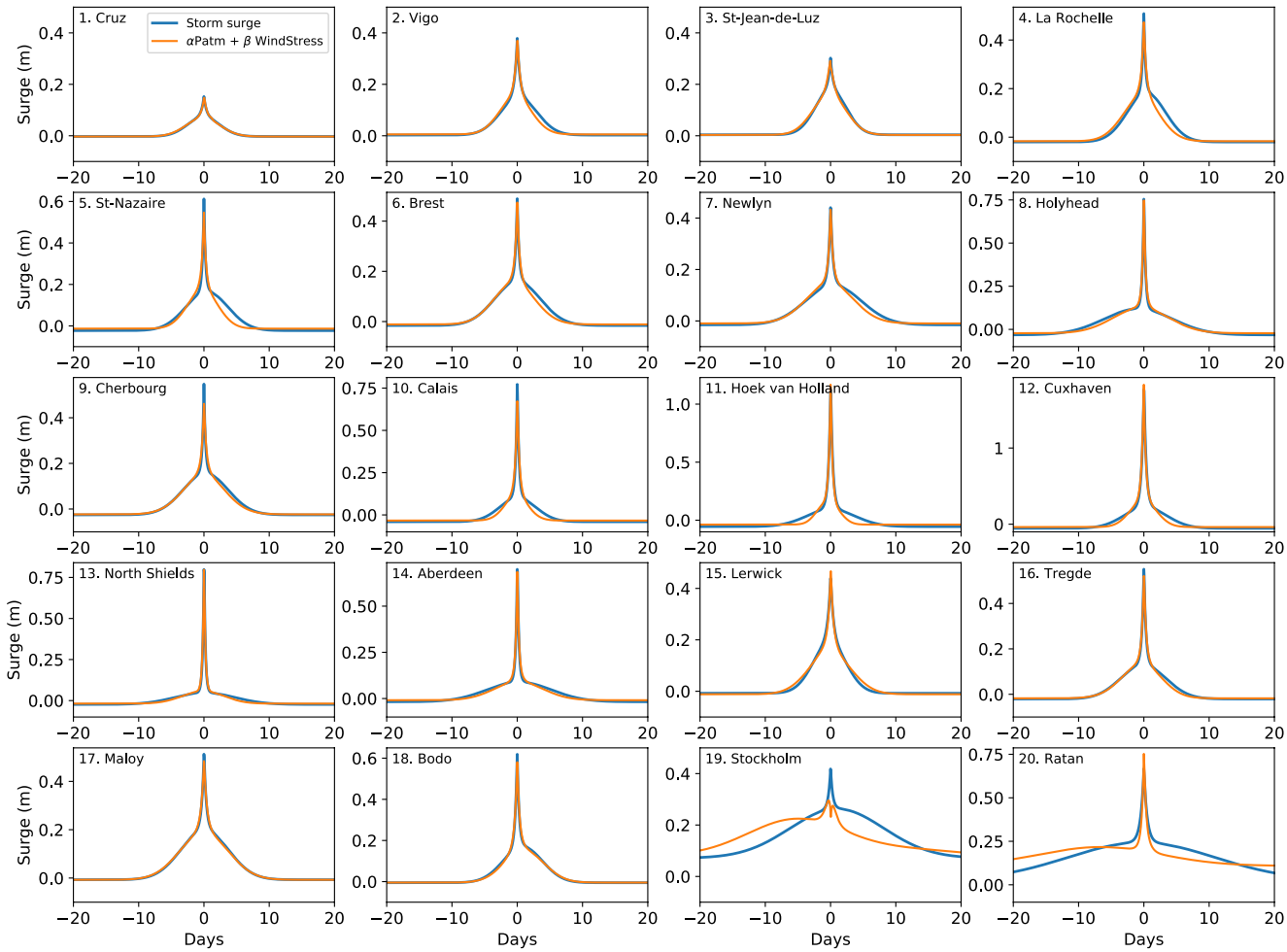

Figure 8. Storm surge event occurring 5 times per winter (in blue) modeled as a multiple linear regression of atmospheric pressure and wind stress events (in orange), at the 20 tide gauges.

water Saint-Venant equations, the wind stress term is divided by the water depth, so the wind stress effect will be enhanced in shallow waters.

5. Discussion

5.1. Shape of a Storm Surge Event, Depending on Its Rarity

The shape of a storm surge event, and associated characteristic parameters, depend greatly on the rarity (or "extremeness") of the storm surge event, that is, how often it occurs per year. Higher amplitudes are naturally expected for storm surge events occurring only twice per winter, rather than 5 times per winter.

Using the proposed ECHAR method, we computed typical shapes of an event occurring 2, 5 and 20 times per winter, at Brest and Cuxhaven (Figure 10). As expected, the peak surge increases with the rarity. (Note that the peak surge corresponds to the sum of the Gaussian and Laplace amplitudes, see Figure 3 for an illustration). At Cuxhaven, the peak surge reaches 2.46 m for a twice per winter event, instead of 1.91 m for a 5 times per winter event. Interestingly, not only the fast-time amplitude a_L increases, but both a_G and a_L increase at the same time (see the differences between the green and orange or blue curves on Figure 10). Finally, at each station, the ratio a_G/a_L is identical, whatever the rarity of the event.

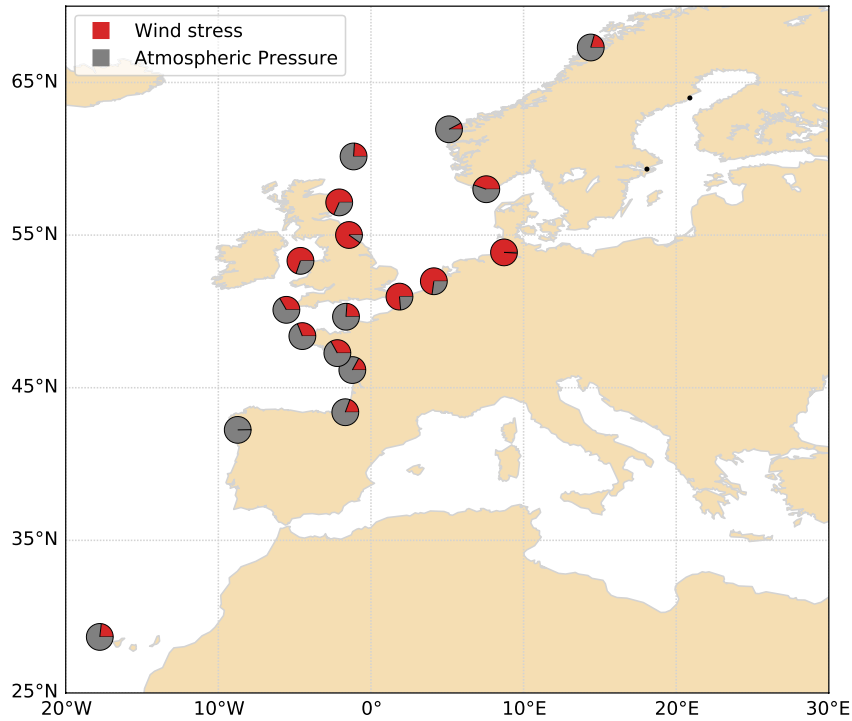

Figure 9. Relative contribution of the wind stress and the atmospheric pressure in a storm surge event occurring 5 times per winter (see Equation 6).

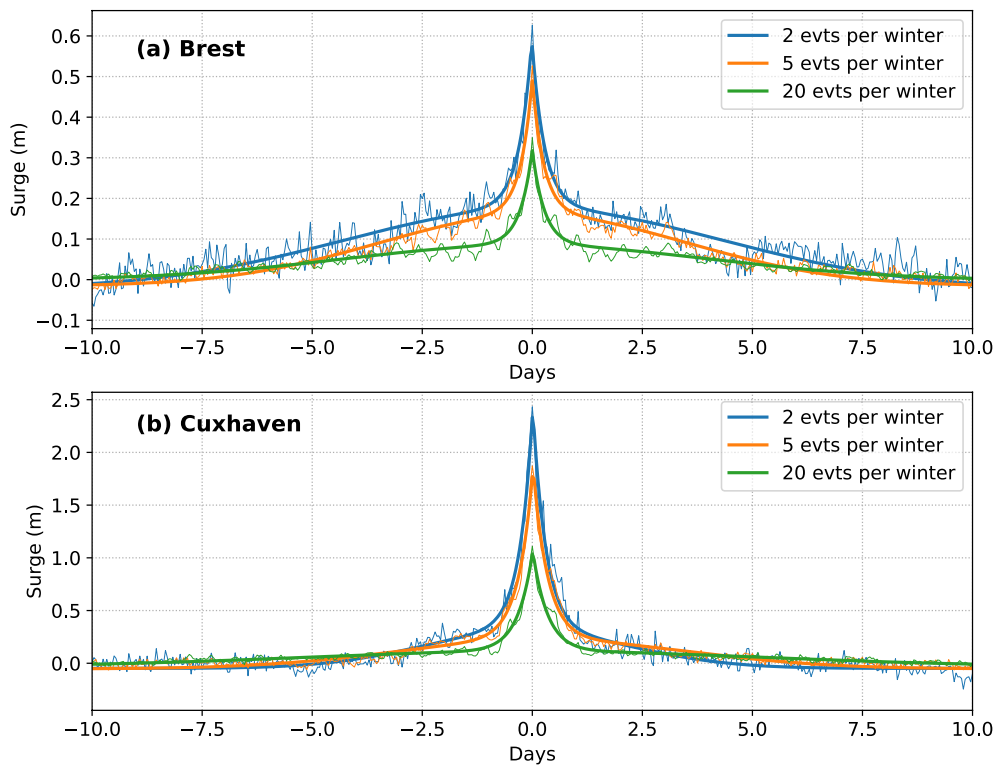

Figure 10. Shape of a storm surge event, depending on how often the event occurs (2, 5, or 20 times a year) at (a) Brest (b) Cuxhaven.

5.2. Storm Surge Processes

We found that storm surge events display a slow-time and a fast-time component, lasting about 16 and 1.7 days, respectively. Each of these component are driven by the atmospheric pressure and the wind stress, respectively. Interestingly, the duration of the fast-time component (which is a proxy for the storm duration) is always smaller than 3 days (it varies from 1.1 day at North Shields to 2.7 days at Ratan, see Table 1). This confirms that a 3-day separation criteria (to ensure independent events, see the Method section) is appropriate along the North-East Atlantic coasts.

Other physical processes emerge from the storm surge signal, and could be further investigated. Three of them are described in the following.

First, at some stations, the fast-time structure peak is shifted with respect to the slow-time structure peak, see for example, station 18 Bodo or station 19 Stockholm on Figure 4. This shift is already present in the atmospheric data, as it is well captured by our model (Equation 5) based on the atmospheric data (see station 18 Bodo on Figure 8). Such a shift suggests that at some stations, strong winds occur before the minimum of atmospheric pressure.

Another aspect is the asymmetry of the curves. At some stations, there is a clear assymmetry between the "flow" and the "ebb" of the fast-time structure, the flow being more steep (or intense) than the ebb (see e.g., station 13 North Shields on Figure 4). This asymmetry could be modeled in the Laplace function (Equation 3), introducing for the flow a σ parameter, and for the ebb a $r * \sigma$ parameter, r being representative of the asymmetry ($r = 1$ when there is no asymmetry, and $r > 1$ when the ebb is longer than the flow). This way, possible asymmetry in curves could be analyzed and further investigated.

A last aspect is the tide-surge interaction. At some stations, oscillations at the frequency of M_2 tide (the main tidal frequency) suggest tide-surge interaction (see e.g., station 2 Vigo on Figure 4, and more details in the Results section). The amplitude of tide-surge interaction can then be easily derived, fitting a cosinus on the storm surge residual (i.e., after removing the Laplace and Gaussian contributions). This is a simple way to estimate directly the amplitude of the tide-surge interaction, compared to more indirect methods (e.g., difference between the maximum skew surge and instantaneous surge, tidal-level or tidal-phase method, Mawdsley and Haigh (2016)). Note that the amplitude of this interaction is modulated by the surge signal: the amplitude is larger at the surge peak, rather than at the beginning of the storm event.

5.3. Possible Applications

The ECHAR method allows to derive time series of typical storm surge events, from sea level observations.

These results have great potential for flood and erosion risk assessment. Flood risk assessment is essential to plan adequate coastal defences and prepare flood mitigation strategies. Flood inundation models typically need storm surges as forcing. Here, we describe three current approaches, before describing the advantages of using the ECHAR time series as forcing. (a) A first approach is to consider a limited number of single parameters to describe the storm surge event, rather than a full time series. For example, Wahl et al. (2016) consider the observed peak surge as a proxy for the storm surge event, when investigating the relationship between six hydrodynamic drivers (surge, tide, significant wave height, wave peak period, storm duration) and erosion and flooding in the northern Gulf of Mexico. For studies based on numerical modeling, which investigate flooding or morphodynamical response during storm-events (e.g., dune erosion using XBeach, Roelvink et al. (2009); Roelvink et al. (2015)), time-varying water levels are used as forcing. (b) A second approach is then to derive hourly sea storm events from a limited number of observed parameters. For example, Santos et al. (2019) derived hourly storm surge time series from only two single values, the peak surge and the storm duration (extracted from existing sea-storm data set, Wahl et al. (2016)). At first order, the shape of the storm surge event was taken as roughly triangular. This led to largely overestimate the intensity of the surge events for tropical storms. More realistic curves (than a triangle) were then preferred. They were computed as the average of the 10 largest events, and then scaled to match the peak surge of each individual event. (c) Another approach is to force the flood or erosion model with simulated storm surge time series (rather than observations). The time series are then extracted from large-scale hydrodynamic models. For example, when assessing the storm impact on a French coastal dune during Xynthia storm, Muller et al. (2017) forced XBeach model with time-varying surges extracted from MARS hydrodynamic model (Lazure & Dumas, 2008). Using storm surges from models (rather than observations) may introduce uncertainties, as storm surges are generally underestimated in numerical models (Muis et al., 2016; Muller et al., 2014).

Possible causes are underestimated strong winds (Pineau-Guillou et al., 2018), inaccurate wind stress formulation (Pineau-Guillou et al., 2020), limited spatial resolution, and non-modeled processes, such as the wave set up (additional surge due to wave dissipation in nearshore areas, Bertin et al. (2015)). Finally, flood risk analysis are often based on a few number of events, for example, 3 storm events in Liu et al. (2016). As storm surges display large interannual and multidecadal variability (Wahl & Chambers, 2015), flooding and erosion estimation will greatly depend on the selected events.

Here, with the ECHAR method, realistic shapes of time-varying storm surges may be used directly as input for flood and erosion studies. The advantages of these inputs are the following: the curves are directly derived from observations, rather than models (which may introduce some underestimates). The shapes, based on Laplace and Gaussian functions, are more realistic than a triangle approach, and show very good agreement with observed storm surge events (on average, RMSE 2 cm). But the most interesting is that we estimated for each typical curve the standard deviation of the surge probability distribution (see the shaded area on Figure 3). Uncertainties on flood and erosion may then be estimated, taking into account as inputs, the typical curve for a given return period (black curve on Figure 3), but also the associated lowest and highest scenarios (envelopes of the gray shaded area on Figure 3).

Another possible application is the generation of artificial storm surge events, with realistic shapes based on the Laplace and Gaussian functions. Again, this large number of sea storm events can be used for flood risk analysis. The first step is to estimate the characteristic parameters (a_G, a_L, σ_G, σ_L) for each individual event, rather than for a typical mean curve (as done in our study). This way, we have the distribution of each characteristic parameter, rather than its mean value. From the distribution of these parameters, the second step is to apply a method close to MacPherson et al. (2019), who stochastically simulated artificial extreme sea level events for the German Baltic Sea coast. Parametric distribution functions are fitted to the observed parameters (in our case, a_G, a_L, σ_G, σ_L). A Gaussian copula is used to preserve the dependence between the observed parameters. Residual water levels are modeled using an autoregressive process. Artificial events are further generated using Monte Carlo simulations, from the previous probability distribution functions. Note that in MacPherson et al. (2019), the shape of storm surge events is triangular (approximated by two second-degree polynomials, as the flow and ebb curves are not necessarily linear), whereas we use Laplace and Gaussian functions (that very well fit the observed events).

Finally, the ECHAR method can be used to investigate changes over time, in the characteristic parameters of extreme surge events. A preliminary study at Cuxhaven (1917–2018) revealed some significant changes over the last century, leading to different shape of storm surge events, between the years 1930 and 1970. Based on the ECHAR method to robustly describe the full dynamics of extreme surge events, further investigations should be conducted to better understand the causes of regional differences, and related changes associated to intensity, size and propagation properties of winter storms.

6. Conclusions

In the North-East Atlantic, we investigated the characteristics of storm surge events at 20 long-term tide gauges, from 1980 up to now. A new method, called ECHAR, is introduced to help characterize extreme events. At each tide gauge, the shape of a typical storm surge event, occurring 5 times per winter, is robustly derived.

Typical storm surge events display a slow-time and a fast-time component. The slow-time component can be approximated with a Gaussian function, while the fast-time one with a Laplace function. Storm surge events are thus reduced to 4 characteristic parameters, that is, amplitude and duration of each slow/fast component.

Characteristic parameters can vary greatly depending on the location. For the slow-time structure, the duration varies from 9 days in the South to 45 days in the North (Baltic Sea), whereas the amplitude is almost identical at all the stations (0.17 ± 0.05 m). On the contrary, for the fast-time structure, the duration is almost identical everywhere (1.7 ± 0.4 days), whereas the amplitude varies greatly, from 0.1 m in the South to 1.6 m in the North Sea. Note that these characteristic parameters depend clearly on the rarity (or "extremeness") of the event, that is, the values will differ for an event occurring 2 rather than 5 times per winter, as chosen in our study.

Typical meteorological events (atmospheric pressure and wind stress) are also found to display a fast-time and slow-time component. The wind stress event is mainly reduced to its fast-time component. This suggests that

the wind stress contributes mostly to the fast-time structure of the storm surge event, whereas the atmospheric pressure contributes to both components. To estimate the relative contribution of the wind stress to the surge event, we modeled a typical storm surge event as a multiple linear regression of an atmospheric pressure event and a wind stress event. The model shows very good performance, except in the Baltic Sea (2 stations among 20). From the model coefficients, we estimated the relative contribution of the wind stress in a storm surge event. The atmospheric pressure is the main driver of storm surge events at most of the stations, whereas the wind stress is the main driver in the North Sea and the Irish Sea. On average, the wind stress contributes to 43% of the storm surge event, and up to 99% in the North Sea. These high values can be explained by the proximity of the storm tracks, and shallow waters environment, which enhance the wind transport effect.

Concerning possible applications, the ECHAR time series of typical storm surge events can be used directly as input for flood and erosion risk assessment. Uncertainties can be estimated, considering the lowest and highest scenarios (envelopes of the gray shaded area on Figure 3). The ECHAR method can also be used to investigate changes over time, in the shape of storm surge events.

Finally, the new ECHAR method, helping to characterize extreme events, is very generic. The method could be applied anywhere else in the global ocean, for example, where storm surges are generated by tropical cyclones, rather than winter extratropical storms. Still, the method can be easily applied to many other time series, such as precipitation, temperature or salinity. The method shall possibly be extended to also help characterize the temporal structure of heat waves (Frölicher & Laufkötter, 2018), known to feature a compound structure of hot days interspersed with cooler breaks, under moderate to high pressure conditions.

Data Availability Statement

The GESLA-3 sea level data set (Caldwell et al., 2015; Haigh et al., 2021; Woodworth et al., 2017) analyzed during the current study is available on the GESLA website, https://gesla787883612.wordpress.com/downloads/. The ERA5 atmospheric hourly data (Hersbach et al., 2018, 2020) were downloaded from the Copernicus Climate Change Service (C3S) Climate Data Store https://doi.org/10.24381/cds.adbb2d47.

Acknowledgments
This research has been supported by the French National Research Agency (ANR) grant ClimEx (ANR-21-CE01-0004).

References

Ade, P. A. R., Ade, P. A. R., Aghanim, N., Armitage-Caplan, C., Arnaud, M., Ashdown, M., et al. (2014). Planck 2013 results. X. HFI energetic particle effects: Characterization, removal, and simulation. *Astronomy & Astrophysics*, *571*, A10. https://doi.org/10.1051/0004-6361/201321577

Allain, D. (2021). TUGOm tidal toolbox. Tech. rep., LEGOS documentation. Retrieved from http://ftp.legos.obs-mip.fr/pub/ecola/tools/ttb.pdf

Bertin, X., Li, K., Roland, A., & Bidlot, J.-R. (2015). The contribution of short-waves in storm surges: Two case studies in the bay of Biscay. *Continental Shelf Research*, *96*, 1–15. https://doi.org/10.1016/j.csr.2015.01.005

Bertin, X., Li, K., Roland, A., Zhang, Y. J., Breilh, J. F., & Chaumillon, E. (2014). A modeling-based analysis of the flooding associated with Xynthia, central Bay of Biscay. *Coastal Engineering*, *94*, 80–89. https://doi.org/10.1016/j.coastaleng.2014.08.013

Calafat, F. M., Wahl, T., Tadesse, M. G., & Sparrow, S. N. (2022). Trends in Europe storm surge extremes match the rate of sea-level rise. *Nature*, *603*(7903), 841–845. https://doi.org/10.1038/s41586-022-04426-5

Caldwell, P. C., Merrifield, M. A., & Thompson, P. R. (2015). Sea level measured by tide gauges from global oceans—The joint archive for sea level holdings (NCEI accession 0019568), version 5.5. [Dataset]. NOAA National Centers for Environmental Information. https://doi.org/10.7289/V5V40S7W

Choi, B. H., Kim, K. O., Yuk, J.-H., & Lee, H. S. (2018). Simulation of the 1953 storm surge in the North Sea. *Ocean Dynamics*, *6*(12), 1759–1777. https://doi.org/10.1007/s10236-018-1223-z

Cid, A., Menéndez, M., Castanedo, S., Abascal, A. J., Méndez, F. J., & Medina, R. (2016). Long-term changes in the frequency, intensity and duration of extreme storm surge events in southern Europe. *Climate Dynamics*, *46*(5–6), 1503–1516. https://doi.org/10.1007/s00382-015-2659-1

Coles, S. (2001). *An introduction to statistical modeling of extreme values*. Springer. https://doi.org/10.1007/978-1-4471-3675-0

Dangendorf, S., Arns, A., Pinto, J. G., Ludwig, P., & Jensen, J. (2016). The exceptional influence of storm "Xaver" on design water levels in the German Bight. *Journal of Climate*, *11*(5), 054001. https://doi.org/10.1088/1748-9326/11/5/054001

Frölicher, T., & Laufkötter, C. (2018). Emerging risks from marine heat waves. *Nature Communications*, *9*(650), 650. https://doi.org/10.1038/s41467-018-03163-6

Haigh, I. D., Marcos, M., Talke, S., Woodworth, P., Hunter, J., Hague, B., et al. (2021). GESLA version 3: A major update to the global higher-frequency sea-level dataset. *Earth ArXiv Preprint*. https://doi.org/10.31223/X5MP65

Haigh, I. D., Nicholls, R. J., & Wells, N. C. (2010). Assessing changes in extreme sea levels: Application to the English Channel, 1900–2006. *Continental Shelf Research*, *30*(9), 1042–1055. https://doi.org/10.1016/j.csr.2010.02.002

Haigh, I. D., Pickering, M. D., Green, J. A. M., Arbic, B. K., Arns, A., Dangendorf, S., et al. (2019). The tides they are a-changin': A comprehensive review of past and future nonastronomical changes in tides, their driving mechanisms and future implications. *Review of Geophysics*, *57*(1), e2018RG000636. https://doi.org/10.1029/2018RG000636

Hellerman, S., & Rosenstein, M. (1983). Normal monthly wind stress over the world ocean. *Journal of Physical Oceanography*, *13*(7), 1093–1104. https://doi.org/10.1175/1520-0485(1983)013<1093:NMWSOT>2.0.CO;2

Hersbach, H., Bell, B., Berrisford, P., Biavati, G., Horányi, A., Muñoz Sabater, J., et al. (2018). ERA5 hourly data on single levels from 1959 to present. [Dataset]. Copernicus Climate Change Service (C3S) Climate Data Store (CDS). https://doi.org/10.24381/cds.adbb2d47

Hersbach, H., Bell, B., Berrisford, P., Hirahara, S., Horányi, A., Muñoz-Sabater, J., et al. (2020). The ERA5 global reanalysis. *Quarterly Journal of the Royal Meteorological Society*, *146*(730), 1999–2049. https://doi.org/10.1002/qj.3803

Horsburgh, K. J., & Wilson, C. (2007). Tide-surge interaction and its role in the distribution of surge residuals in the North Sea. *Journal of Geophysical Research*, *112*(C8), C08003. https://doi.org/10.1029/2006JC004033

Idier, D., Dumas, F., & Muller, H. (2012). Tide-surge interaction in the English Channel. *Natural Hazards and Earth System Sciences*, *12*, 3709–3718. https://doi.org/10.5194/nhess-12-3709-2012

IPCC. (2021). In V. Masson-Delmotte, P. Zhai, A. Pirani, S. L. Connors, C. Péan, S. Berger, et al. (Eds.), *Climate change 2021: The physical science basis. Contribution of working group I to the sixth assessment report of the intergovernmental panel on climate change*. Cambridge University Press.

Lazure, P., & Dumas, F. (2008). An external–internal mode coupling for a 3D hydrodynamical model for applications at regional scale (MARS). *Advances in Water Resources*, *31*(2), 233–250. https://doi.org/10.1016/j.advwatres.2007.06.010

Liu, Q., Ruan, C., Zhong, S., Li, J., Yin, Z., & Lian, X. (2016). Risk assessment of storm surge disaster based on numerical models and remote sensing. *International Journal of Applied Earth Observation and Geoinformation*, *68*, 20–30. https://doi.org/10.1016/j.jag.2018.01.016

MacPherson, L. R., Arns, A., Dangendorf, S., Vafeidis, A. T., & Jensen, J. (2019). A stochastic extreme sea level model for the German Baltic Sea coast. *Journal of Geophysical Research: Oceans*, *124*(3), 2054–2071. https://doi.org/10.1029/2018JC014718

Marcos, M., Calafat, F. M., Berihuete, Á., & Dangendorf, S. (2015). Long-term variations in global sea level extremes. *Journal of Geophysical Research: Oceans*, *120*(12), 8115–8134. https://doi.org/10.1002/2015JC011173

Marcos, M., & Woodworth, P. L. (2017). Spatiotemporal changes in extreme sea levels along the coast of the North Atlantic and the Gulf of Mexico. *Journal of Geophysical Research: Oceans*, *122*(9), 7031–7048. https://doi.org/10.1002/2017JC013065

Mawdsley, R. J., & Haigh, I. D. (2016). Spatial and temporal variability and long-term trends in skew surges globally. *Frontiers in Marine Science*, *3*. https://doi.org/10.3389/fmars.2016.00029

Menéndez, M., & Woodworth, P. L. (2010). Changes in extreme high water levels based on a quasi-global tide-gauge data set. *Journal of Geophysical Research*, *115*(C10), C10011. https://doi.org/10.1029/2009JC005997

Muis, S., Verlaan, M., Winsemius, H. C., Aerts, J. C., & Ward, P. J. (2016). A global reanalysis of storm surges and extreme sea levels. *Nature Communications*, *7*(1), 11969. https://doi.org/10.1038/ncomms11969

Muller, H., Pineau-Guillou, L., Idier, D., & Ardhuin, F. (2014). Atmospheric storm surge modeling methodology along the French (Atlantic and English Channel) coast. *Ocean Dynamics*, *64*(11), 1671–1692. https://doi.org/10.1007/s10236-014-0771-0

Muller, H., van Rooijen, A., Idier, D., Pedreros, R., & Rohmer, J. (2017). Assessing storm impact on a French coastal dune system using morpho-dynamic modeling. *Journal of Coastal Research*, *33*(2), 254–272. https://doi.org/10.2112/JCOASTRES-D-15-00102

Pineau-Guillou, L., Ardhuin, F., Bouin, M.-N., Redelsperger, J.-L., Chapron, B., Bidlot, J.-R., & Quilfen, Y. (2018). Strong winds in a coupled wave–atmosphere model during a North Atlantic storm event: Evaluation against observations. *Quarterly Journal of the Royal Meteorological Society*, *144*(711), 317–332. https://doi.org/10.1002/qj.3205

Pineau-Guillou, L., Bouin, M.-N., Ardhuin, F., Lyard, F., Bidlot, J.-R., & Chapron, B. (2020). Impact of wave-dependent stress on storm surge simulations in the North Sea: Ocean model evaluation against in situ and satellite observations. *Ocean Modelling*, *154*, 101694. https://doi.org/10.1016/j.ocemod.2020.101694

Pineau-Guillou, L., Lathuiliere, C., Magne, R., Louazel, S., Corman, D., & Perherin, C. (2012). Sea levels analysis and surge modelling during storm Xynthia. *European Journal of Environmental and Civil Engineering*, *16*(8), 943–952. https://doi.org/10.1080/19648189.2012.676424

Pineau-Guillou, L., Lazure, P., & Wöppelmann, G. (2021). Large-scale changes of the semidiurnal tide along North Atlantic coasts from 1846 to 2018. *Ocean Science*, *17*(1), 17–34. https://doi.org/10.5194/os-17-17-2021

Pugh, D., & Woodworth, P. (2014). *Sea-level science: Understanding tides, surges, tsunamis and mean sea-level changes*. Cambridge University Press.

Reinert, M., Pineau-Guillou, L., Raillard, N., & Chapron, B. (2021). Seasonal shift in storm surges at Brest revealed by extreme value analysis. *Journal of Geophysical Research: Oceans*, *126*(12), e2021JC017794. https://doi.org/10.1029/2021JC017794

Roelvink, D., Reniers, A., van Dongeren, A., van Thiel de Vries, J., McCall, R., & Lescinski, J. (2009). Modelling storm impacts on beaches, dunes and barrier islands. *Coastal Engineering*, *56*(11), 1133–1152. https://doi.org/10.1016/j.coastaleng.2009.08.006

Roelvink, D., van Dongeren, A., McCall, R., Hoonhout, B., van Rooijen, A., van Geer, P., et al. (2015). XBeach technical reference: Kingsday release [Technical Report]. https://doi.org/10.13140/RG.2.1.4025.6244

Roustan, J.-B., Pineau-Guillou, L., Chapron, B., Reinert, M., & Raillard, N. (2022). Shift of the storm surge season in Europe due to climate variability. *Scientific Reports*, *12*(8210), 8210. https://doi.org/10.1038/s41598-022-12356-5

Santos, V. M., Wahl, T., Long, J. W., Passeri, D. L., & Plant, N. G. (2019). Combining numerical and statistical models to predict storm-induced dune erosion. *J. Geophys. Res.Earth Surface*, *124*(7), 1817–1834. https://doi.org/10.1029/2019JF005016

Simon, B. (2007). *La marée océanique côtière*. Institut Océanographique Ed. Retrieved from https://iho.int/iho_pubs/CB/C-33/C-33_maree_simon_fr.pdf

Simon, B. (2013). *Coastal tides*. Institut Océanographique Ed. Retrieved from https://iho.int/iho_pubs/CB/C-33/C-33_maree_simon_en.pdf

Talke, S. A., Orton, P., & Jay, D. A. (2014). Increasing storm tides in New York Harbor, 1844–2013. *Geophysical Research Letters*, *41*(9), 3149–3155. https://doi.org/10.1002/2014GL059574

Vousdoukas, M. I., Voukouvalas, E., Annunziato, A., Giardino, A., & Feyen, L. (2016). Projections of extreme storm surge levels along Europe. *Climate Dynamics*, *47*(9–10), 3171–3190. https://doi.org/10.1007/s00382-016-3019-5

Wahl, T., & Chambers, D. P. (2015). Evidence for multidecadal variability in us extreme sea level records. *Journal of Geophysical Research: Oceans*, *120*(3), 1527–1544. https://doi.org/10.1002/2014JC010443

Wahl, T., Plant, N. G., & Long, J. W. (2016). Probabilistic assessment of erosion and flooding risk in the northern Gulf of Mexico. *Journal of Geophysical Research: Oceans*, *121*(5), 3029–3043. https://doi.org/10.1002/2015JC011482

Wolf, J., & Flather, R. (2005). Modelling waves and surges during the 1953 storm. *Philosophical Transactions of the Royal Society A*, *363*(1831), 1359–1375. https://doi.org/10.1098/rsta.2005.1572

Woodworth, P. L., Hunter, J. R., Marcos, M., Caldwell, P., Menéndez, M., & Haigh, I. (2017). Towards a global higher-frequency sea level dataset. *Geoscience Data Journal*, *3*(2), 50–59. https://doi.org/10.1002/gdj3.42